

Surface wave tomography from microseisms in Southern California

Karim G. Sabra, Peter Gerstoft, Philippe Roux, and W. A. Kuperman

Marine Physical Laboratory of the Scripps Institution of Oceanography, University of California, San Diego, La Jolla, California, USA

Michael C. Fehler

Los Alamos National Laboratory, Los Alamos, New Mexico, USA

Received 5 April 2005; revised 23 May 2005; accepted 9 June 2005; published 26 July 2005.

[1] Since it has already been demonstrated that point-to-point seismic propagation Green Functions can be extracted from seismic noise, it should be possible to image Earth structure using the ambient noise field. Seismic noise data from 148 broadband seismic stations in Southern California were used to extract the surface wave arrival-times between all station pairs in the network. The seismic data were then used in a simple, but densely sampled tomographic procedure to estimate the surface wave velocity structure within the frequency range of 0.1–0.2 Hz for a region in Southern California. The result compares favorably with previous estimates obtained using more conventional and elaborate inversion procedures. This demonstrates that coherent noise field between station pairs can be used for seismic imaging purposes. **Citation:** Sabra, K. G., P. Gerstoft, P. Roux, W. A. Kuperman, and M. C. Fehler (2005), Surface wave tomography from microseisms in Southern California, *Geophys. Res. Lett.*, 32, L14311, doi:10.1029/2005GL023155.

1. Introduction

[2] Imaging the structure of the Earth traditionally uses the measured response from energetic active controlled sources (e.g. explosions or seismic vibrators) or specific earthquakes in order to infer the arrival-times of the local Time Domain Green's Function (TDGF) [Aki and Richards, 1980]. On the other hand, an estimate of the TDGF between pairs of seismic stations can be extracted from the coherent, deterministic arrival-times obtained from the time-derivative of the Noise Cross-correlation Function (NCF) [Rickett and Claerbout, 1999; Weaver and Lobkis, 2001] (Figure 1). This TDGF estimated from the noise field alone includes all tensor components of the Green's function. The resulting waveforms can be used to infer Earth structure from existing worldwide networks of broadband seismic stations, without relying on active sources or identifiable earthquakes. In this article, we apply the above procedure to noise data collected on the 148 broadband stations of the Southern California network sampled at 20 Hz to invert for the group velocity surface wave structure in the frequency range of 0.1–0.2 Hz of the area using a classical tomographic approach. During the revision of the paper, it came to our attention that Shapiro *et al.* [2005] also performed tomographic inversion of the Southern California using TDGF estimated from noise. Our approach differs on several points from theirs: 1) We use the time-derivative of NCF (and

not the NCF directly) as an estimate of the TDGF, 2) The influence of large events are reduced by clipping of the amplitudes (and not by using the one bit information), 3) A denser seismic array of 148 stations instead of 62 was used and a smaller covered area results in a higher path coverage and thus a higher tomographic resolution across a finer grid. In addition, we present further evidence that favors the oceanic origin of the recorded microseisms for the [0.1–0.2 Hz] band based on the orientation of the station pairs relative to the coastline and the corresponding signal-to-noise ratio of the estimated TDGF.

[3] Experimental and theoretical confirmation have shown that the arrival-time structure of the TDGF can be estimated from the NCF in various environments and frequency ranges of interest: helioseismology [Rickett and Claerbout, 1999], ultrasonics [Weaver and Lobkis, 2001, 2003, 2004; Larose *et al.*, 2004; Malcolm *et al.*, 2004], underwater acoustics [Roux *et al.*, 2004; Sabra *et al.*, 2005a], and seismology [Shapiro and Campillo, 2004; Snieder, 2004; Wapenaar, 2004; Sabra *et al.*, 2005b; Shapiro *et al.*, 2005]. The physical process underlying this noise cross-correlation technique is similar for all these environments. Initially, the small coherent component of the noise field at each receiver is buried in spatially and temporally incoherent field produced by the distribution of noise sources. The coherent wavefronts emerge from a correlation process that accumulates contributions over time from noise sources whose propagation path passes through both receivers. Based on analytic derivations for specific propagation models [Snieder, 2004; Weaver and Lobkis, 2004; Wapenaar, 2004; Roux *et al.*, 2005] and following the discussions in Sabra *et al.* [2005b] (equations 1 and 2), the time-derivative of the NCF is proportional to the sum of the negative TDGF and the time-reversed TDGF for an isotropic noise source distribution. The derivative of the NCF is an anti-symmetric function with respect to time, the NCF itself being a symmetric function.

[4] However the seismic noise field might not be isotropic when dominated by directional noise sources, such as ocean microseisms [Bromirsky and Duennebieer, 2002]. And the station pair orientation will matter. Indeed to the first order for a weakly scattering medium (e.g. the Earth crust but not a random cavity), the regions of constructive interference for the noise sources contributing to the time-averaged NCF are roughly located in the two broad end-fire beams [Snieder, 2004; Roux *et al.*, 2004; Sabra *et al.*, 2005a]. Noise sources located outside of these end-fire beams typically have a weaker contribution to the NCF. Thus, for a weakly scattering medium and an anisotropic

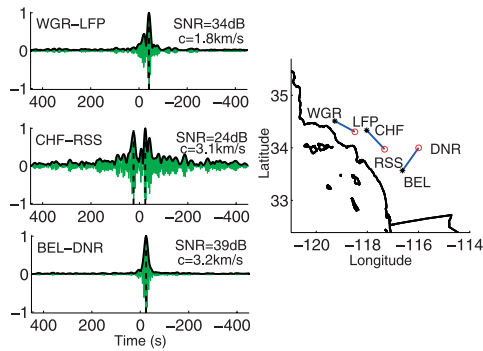


Figure 1. Derivative of the time-averaged noise cross-correlation functions (NCF) in the frequency band [0.1–0.2 Hz] for three seismic station pairs, showing a surface-wave arrival (station 1 is indicated by a star and station 2 by a circle). The arrival-time (dashed) is determined by the maximum of the envelope of pulse (heavy line). Corresponding signal-to-noise ratio SNR and estimated surface wave group velocity c are indicated for each waveform.

noise sources distribution, coherent waveforms may not emerge easily from the NCF if the station pair is oriented perpendicular to the main propagation path of the noise sources.

2. Data Processing

[5] The cross-correlation technique was applied to seismic recordings collected on the vertical component of 148 broadband stations of the Southern California seismic network for a continuous recording period (1–18 July 2004) [Sabra et al., 2005b]. Data processing is described in details in Sabra et al. [2005b]. Data clipping is used to reduce the influence of episodic energetic events (e.g. earthquakes) on the cross-correlation. A specific amplitude threshold was computed for each station before clipping the recordings instead of using a simple but rougher one-bit truncation [Larose et al., 2004; Shapiro et al., 2005]. The NCFs of the amplitude-truncated recordings were computed in the frequency band [0.1–0.2 Hz] centered on the maximum of the ocean microseisms and atmospheric disturbances spectra [Aki and Richards, 1980, chap. 10; Bromirsky and Duennebier, 2002; Shapiro et al., 2005]. In this frequency band, seismic noise propagating over long distances is typically dominated by surface waves; thus, the time-derivative of the NCF reduces to the surface-wave portion of the TDGF between two stations of this network [Shapiro and Campillo, 2004; Sabra et al., 2005b; Shapiro et al., 2005].

3. Experimental Results

[6] Figure 1 illustrates the spatial variations of the waveforms estimated from the time-derivative of the NCFs. Since the waveforms are issued from a correlation process, the arrival-time (and thus the group velocity) was determined by the maximum of the of pulse envelope (i.e. the center of the pulse) and not by the first break as usually done for earthquake arrivals. Given the network's proximity to the Pacific coast, the directionality of the seismic noise, dominated by ocean microseisms around [0.1–0.2 Hz],

yields mostly one-sided NCFs for station pairs oriented perpendicular to the coast (see Figure 1 and Sabra et al. [2005b]). The inter-station distance 75 km is similar for the three pairs shown in Figure 1 but they are located in geologically different areas of Southern California and have different orientation thus yielding waveforms with different arrival-times. Some station pairs (e.g. CHF-RSS in Figure 1) have an almost symmetric arrival time structure. For each waveform, the signal-to-noise ratio SNR is defined as the ratio of the maximum of the envelope of the main surface-wave arrival (Figure 1) and the standard deviation for an incoherent noise-only time-window, (selected as $400 \text{ s} \leq |t| \leq 450 \text{ s}$).

[7] Figure 2 indicates the spatial dependency of the SNR (in dB) on the bearing angle of the station pair. Scattering from heterogeneities [Hennino et al., 2001] and geometric effects (e.g. such as reflections from the edge of a basin [Aki and Richards, 1980]) randomizes the noise field and thus partially redistributes the ocean microseism wavefield making it more uniform. Some station pairs oriented to the coast have relatively symmetric NCFs with a sufficiently high SNR (e.g. CHF-RSS on Figure 1) and this may be due to scattered ocean noise propagating along their station axis. However, NCF for station pairs oriented perpendicular to the coast emerge overall more reliably and have a higher SNR than for station pairs oriented parallel to the coastline (Figure 2). Thus, to ensure that the arrival-time of the surface wave part of the TDGF is correctly identified, only the time-derivative of NCFs between station pairs having a SNR > 15 dB were used, a slightly higher threshold than used by Shapiro et al. [2005] and a separation distance larger than 24 km (multiple arrivals were sometimes present for shorter distances based on NCF waveform inspection). This threshold selected 2809 arrival-times measurements with the highest SNR corresponding to inter-station distance from 24 km to 512 km.

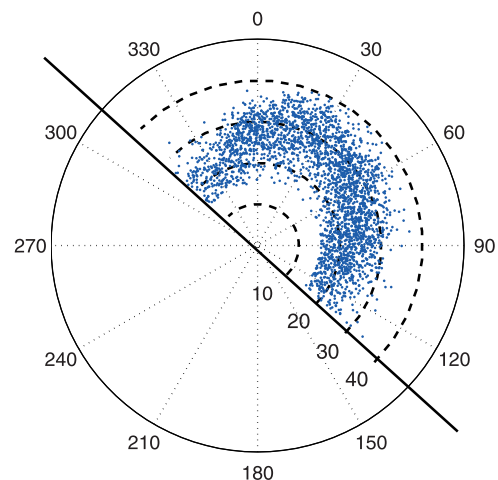


Figure 2. Distribution of the SNR (above 15 dB) of the time-derivative of the NCF (averaged over 18 days) vs. the bearing angle of all station pairs (North is 0°). The coastline orientation is approximated by a straight line with a bearing of 135° . The 10 to 40 dB SNR level are indicated by dashed semi-circles. The overall SNR of the NCF for station pairs oriented perpendicular to the coast (i.e. bearing angle between 10° and 80°) is higher than for the station pair oriented parallel to the coastline.

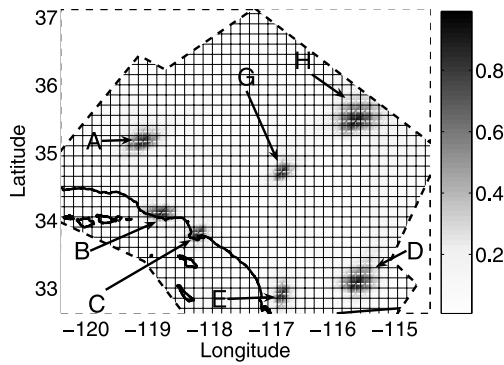


Figure 3. Lateral resolution kernels at seven locations (A: San Joaquin Valley, B: Ventura basin, C: Los Angeles basin, D: Salton Sea, E: Peninsular ranges, G: Mojave Desert, H: East of the Great Basin).

[8] The Southern California region is divided into 13×16 km constant group velocity cells for the tomographic inversion, as indicated in Figure 3. The propagation paths are assumed to be straight rays. If \mathbf{T} is the data vector composed of the arrival-time residuals, \mathbf{S} is the model vector composed of the group slowness variations of each grid cell and assuming a simple linear model, the inversion problem reduces to $\mathbf{T} = \mathbf{KS}$ [Tarantola, 1987; Menke, 1989]. \mathbf{K} is the forward mapping matrix (or kernel) indicating for each particular straight ray its path length across each crossed cell grids. The group velocity value is assigned to the full rectangular cell not only its center.

[9] An averaged arrival-time measurement-error of $\sigma_T = 2$ s is assumed (and thus a simple diagonal measurement-error covariance matrix), in agreement with the frequency-bandwidth resolution. The elements of the a priori error covariance matrix of the cell slownesses Σ_s are:

$$\Sigma_s(i,j) = \sigma_s^2 \exp(-D_{i,j}/L), \quad (1)$$

where $\sigma_s = \sigma_c/c_0^2$, $c_0 = 2.8$ km/s is average regional group velocity, and σ_c is set to 0.15 km/s based on group-velocity measurements from 1.1 to 4.5 km/s. $D_{i,j}$ is the distance (in kilometers) between the center of the i th and j th grid cell and L is a smoothness scale set to 30 km so that the smoothing extends over 2 grid cells [Tarantola, 1987; Rodgers, 2000].

[10] Figure 3 displays lateral resolution kernels for the tomographic inversion procedure [Tanimoto and Sheldrake, 2002]. The target location is given by a unit amplitude cell for each of the seven locations (a–f). The typical resolution length is 30 km, corresponding to the smoothness scale. On the edges of the domain (e.g. label D), the resolutions kernels extend over 50 km. Figure 4 shows the diagonal of the model resolution matrix. Values close to one indicate best resolution and correspond to regions with dense paths coverage.

[11] Using a homogeneous starting model based on the a priori average regional group velocity $c_0 = 2.8$ km/s, the inversion is then performed on the arrival-time residuals. Figure 5 shows the resulting velocity map of the maximum a posteriori solution [Tarantola, 1987; Menke, 1989]. This map produces a residuals variance reduction of 50% relative to residuals for the homogenous model. There is a good

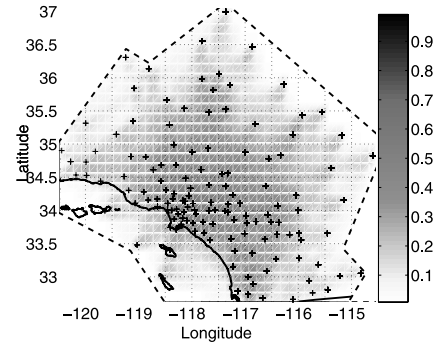


Figure 4. Diagonal of the resolution matrix for the inversion model keeping only the 2809 station pairs having an SNR > 15 dB. Crosses indicate the location of the 148 seismic stations of the Southern California seismic network. The area used from tomographic inversion is indicated by dashed lines.

correlation between the group velocity obtained from the surface wave inversion map (Figure 5) and several geological features of the Southern California [Jennings, 1977; Shapiro et al., 2005]. Slow surface wave velocity regions (labels A–D) correspond to sedimentary basins. Fast group velocities characterize mountain ranges (labels E (Peninsular Ranges) and F (Sierra Nevada)). The main imaged geologic units are consistent with Shapiro et al. [2005]. However a greater velocity contrast is observed 1) along the San Andreas Fault and 2) on the East of the Great Basin and the Mojave Desert, along a low velocity zone extending approximately from (117W, 36N) to (116W, 33.5N).

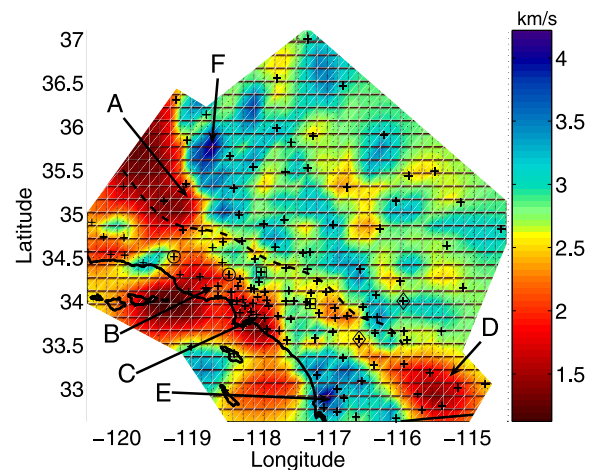


Figure 5. Velocity map corresponding to the maximum a posteriori solution for the tomographic inversion scheme. Low resolution area (determined from Figure 4) were masked. The main sedimentary basins (A: San Joaquin Valley, B: Ventura basin, C: Los Angeles basin, D: Salton Sea) and mountain ranges (E: Peninsular Ranges, F: Sierra Nevada) are indicated. A dashed-line indicates part of the San-Andreas fault. The 148 seismic stations are indicated with crosses. The 3 stations pairs shown in Figure 1 are highlighted using a circle (pair WGR-LFP), square (pair CHF-RSS) or diamond (pair BEL-DNR) symbol.

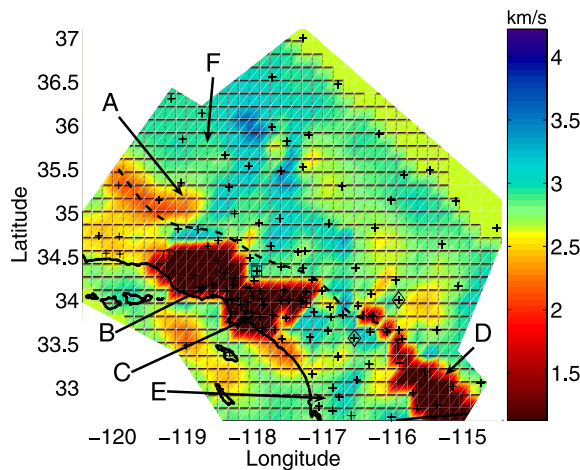


Figure 6. Estimated map of the Rayleigh wave group velocity at 7.5 s constructed from dispersion analysis [Herrmann, 2002] based on a 3D velocity model for the Southern California region [Kohler et al., 2003]. Geological structures labels and velocity color scale are similar to Figure 5.

[12] This tomographic map also agrees quantitatively with an estimated group velocity map computed from dispersion curve analysis at 7.5 s [Herrmann, 2002] based on a previous 3D model for P and S wave velocity profiles in the Southern California region [Kohler et al., 2003] (Figure 6). The average background group velocity and main geological units in Figure 6 agree with those in Figure 5, but overall the image resolution is lower. The very low group velocity for the sedimentary basins (A, B and D) predicted by the 3D model (around 0.5 km/s) differ from Figure 5.

4. Conclusion

[13] The time domain Greens function (TDGF) was estimated from cross-correlation of continuous noise recordings dominated by ocean microseisms in the frequency band [0.1–0.2 Hz]. A high-resolution tomographic map for surface wave group velocity in Southern California was constructed using the estimated TDGF with signal-to-noise ratios larger than 15 dB.

[14] **Acknowledgments.** Funding was provided by the UCSD/LANL CARE-program. Data came from the Southern California Earthquake Center. We thank the three reviewers for constructive comments and B. Cornuelle for helpful discussions about tomographic methods. We thank George Randall and Monica Maceira for help with dispersion calculations.

References

Aki, K., and P. G. Richards (1980), *Qualitative Seismology*, W. H. Freeman, New York.
 Bromirsky, P. D., and F. K. Duennebier (2002), The near-coastal microseism spectrum: Spatial and temporal wave climate relationships, *J. Geophys. Res.*, *107*(B8), 2166, doi:10.1029/2001JB000265.

Hennino, R., N. Trégourès, N. M. Shapiro, L. Margerin, M. Campillo, B. A. van Tiggelen, and R. L. Weaver (2001), Observation of equipartition of seismic waves, *Phys. Rev. Lett.*, *87*, 3447–3450.
 Herrmann, R. (2002), Computer programs in seismology, version 3.15, St. Louis Univ., St. Louis, Mo.
 Jennings, C. W. (1977), Geologic map of California, *Map 2*, Div. of Mines and Geol., Sacramento, Calif.
 Kohler, M. D., H. Magistrale, and R. W. Clayton (2003), Mantle heterogeneities and the SCEC Reference Three-Dimensional Seismic Velocity Model, version 3, *Bull. Seismol. Soc. Am.*, *93*, 757–774.
 Larose, E., A. Derode, M. Campillo, and M. Fink (2004), Imaging from one-bit correlations of wideband diffuse wavefields, *J. Appl. Phys.*, *95*, 8393–8399.
 Malcolm, A. E., J. A. Scales, and B. A. van Tiggelen (2004), Extracting the Green function from diffuse, equipartitioned waves, *Phys. Rev. E*, *70*, 015601, doi:10.1103/PhysRevE.70.015601.
 Menke, W. (1989), *Geophysical Data Analysis: Discrete Inverse Theory*, Elsevier, New York.
 Rickett, J., and J. Claerbout (1999), Acoustic daylight imaging via spectral factorization: Helioseismology and reservoir monitoring, *Leading Edge*, *18*, 957–960.
 Rodgers, C. D. (2000), *Inverse Methods for Atmospheric Sounding Theory and Practice*, World Sci., Hackensack, N. J.
 Roux, P., W. A. Kuperman, and the NPAL Group (2004), Extracting coherent wavefronts from acoustic ambient noise in the ocean, *J. Acoust. Soc. Am.*, *116*, 1995–2003.
 Roux, P., K. G. Sabra, W. A. Kuperman, and A. Roux (2005), Ambient noise cross-correlation in free space: Theoretical approach, *J. Acoust. Soc. Am.*, *117*, 79–84.
 Sabra, K. G., P. Roux, and W. A. Kuperman (2005a), Arrival-time structure of the time-averaged ambient noise cross-correlation function in an oceanic waveguide, *J. Acoust. Soc. Am.*, *117*, 164–174.
 Sabra, K. G., P. Gerstoft, P. Roux, W. A. Kuperman, and M. C. Fehler (2005b), Extracting time-domain Greens function estimates from ambient seismic noise, *Geophys. Res. Lett.*, *32*, L03310, doi:10.1029/2004GL021862.
 Shapiro, N. M., and M. Campillo (2004), Emergence of broadband Rayleigh waves from correlations of the ambient seismic noise, *Geophys. Res. Lett.*, *31*, L07614, doi:10.1029/2004GL019491.
 Shapiro, N. M., M. Campillo, L. Stehly, and M. H. Ritzwoller (2005), High-resolution surface-wave tomography from ambient seismic noise, *Science*, *29*, 1615–1617.
 Snieder, R. (2004), Extracting the Green's function from the correlation of coda waves: A derivation based on stationary phase, *Phys. Rev. E*, *69*, 046610, doi:10.1103/PhysRevE.69.046610.
 Tanimoto, T., and K. P. Sheldrake (2002), Three-dimensional S-wave velocity structure in Southern California, *Geophys. Res. Lett.*, *29*(8), 1223, doi:10.1029/2001GL013486.
 Tarantola, A. (1987), *Inverse Problem Theory*, Elsevier, New York.
 Wapenaar, K. (2004), Retrieving the elastodynamic Green's function of an arbitrary inhomogeneous medium by cross correlation, *Phys. Rev. Lett.*, *93*, 254301, doi:10.1103/PhysRevLett.93.254301.
 Weaver, R. L., and O. I. Lobkis (2001), Ultrasonics without a source: Thermal fluctuation correlations at MHz frequencies, *Phys. Rev. Lett.*, *87*, 134301, doi:10.1103/PhysRevLett.87.134301.
 Weaver, R. L., and O. I. Lobkis (2003), Elastic wave thermal fluctuations, ultrasonic waveforms by correlation of thermal photons, *J. Acoust. Soc. Am.*, *113*, 2611–2621.
 Weaver, R. L., and O. I. Lobkis (2004), Diffuse fields in open systems and the emergence of the Green's function, *J. Acoust. Soc. Am.*, *116*, 2731–2734.

M. C. Fehler, Los Alamos National Laboratory, Los Alamos, NM 87545, USA.

P. Gerstoft, W. A. Kuperman, P. Roux, and K. G. Sabra, Marine Physical Laboratory of the Scripps Institution of Oceanography, University of California, San Diego, La Jolla, CA 92093-0238, USA. (ksabra@mpl.ucsd.edu)